Heat flux induced blueshift of dominant phonon wavelength and its impact on thermal conductivity

Aymeric Ramiere, Sebastian Volz, and Jay Amrit

Heat flux induced blueshift of dominant phonon wavelength and its impact on thermal conductivity

Aymeric Ramiere,[1,2] Sebastian Volz,[3] and Jay Amrit[1,a]

[1]*Laboratoire d'Informatique pour la Mécanique et les Sciences de l'Ingénieur (LIMSI/CNRS), UPR 3251, Université Paris Sud, Rue John von Neumann, 91403 Orsay, France*
[2]*Laboratory for Integrated MicroMechatronic Systems, Institute of Industrial Science (LIMMS/CNRS-IIS), UMI 2820, The University of Tokyo, 153-8505 Tokyo, Japan*
[3]*Laboratoire d'Energétique Moléculaire et Macroscopique, Combustion (EM2C/CNRS), UPR 288, CentraleSupélec, Université Paris-Saclay, 92295 Chatenay-Malabry, France*

The concept of dominant phonon wavelength is investigated in systems submitted to a heat flux at low temperatures. Using spectral energy distributions, a treatment of two-dimensional and three-dimensional structures is conducted in parallel. We demonstrate a significant reduction of the dominant phonon wavelength, up to 62%, due to a displacement of the phonon spectrum towards higher frequencies in presence of a heat flux. We name this phenomenon *blueshift* effect. A formula is provided to directly calculate the corrected dominant phonon wavelength. We illustrate the impact of the *blueshift* effect by showing that a temperature gradient of 10% at 4K yields a 20% reduction in the thermal conductivity. Therefore, ignoring the *blueshift* effect in a thermal model can notably alter the physical interpretation of measurements. The results suggest that an appropriate heat flux environment can improve thermo-electric device performances. © *2017 Author(s). All article content, except where otherwise noted, is licensed under a Creative Commons Attribution (CC BY) license (http://creativecommons.org/licenses/by/4.0/).* [http://dx.doi.org/10.1063/1.4971275]

I. INTRODUCTION

The necessity to control heat propagation in ceaselessly smaller devices has been sustaining the growing interest in nanoscale thermal transport for the past two decades.[1–3] Today, the electronic technologies are based on the Silicon in the frame of three-dimensional (3D) thermal physics. Meanwhile, two-dimensional (2D) materials are being intensively studied and exhibit remarkable heat transport properties.[4–6]

In general, thermal conduction properties depend on temperature and phonons frequencies. At a given temperature, a broad phonon frequency spectrum, ranging from GHz to THz,[7,8] is excited, leading to phonon wavelengths ranging from μm to nm, respectively. Except by simulations,[9–11] it is not possible to experimentally track the specific contribution of each of these modes yet. However, it is common to extract a global behavior by using the notion of a dominant phonon angular frequency ω_d defined as

$$\hbar\omega_d = \alpha k_B T, \tag{1}$$

where $\hbar$ refers to the reduced Planck constant, k_B the Boltzmann constant, T the temperature and α a dimensionless factor that we name the *dominant coefficient*. ω_d is often converted into the dominant phonon wavelength (DPW) λ_d which is used at many occasions.[12–28]

The DPW represents a crucial and convenient parameter to immediately assess the physics of phonons without having to conduct sophisticated and time consuming simulations. It is strongly correlated to the heat propagation properties in a material. Also, the DPW can be compared to the system dimensions in order to evaluate the presence of coherence effects[29,30] and to determine the specularity parameter for the phonon-surface roughness interactions.[18]

[a]jay.amrit@limsi.fr

Despite its important role, several definitions of the DPW coexist in the literature differing by the *dominant coefficient* α. For 3D materials, four values of α can be found. First,[12–15] $\alpha = 4.25$, which finds its origin in measurements conducted by Pohl.[31] A second commonly[16–18] applied coefficient is $\alpha = 2.82$, which is often attributed to Ziman.[16] In the context of thermal contact resistances with superfluid Helium,[19–22] the peak of the specific heat is utilized to find $\alpha = 3.83$. Furthermore, some authors[23–26] omit the factor α and simply set $\hbar\omega_d \approx k_B T$, arguing that an order of magnitude accuracy remains relevant, which may certainly be true in some cases. For 2D materials, fewer studies are available up to now, but the usual value is consistent with[27,28] $\alpha_{2D} \approx 1.6$ given by Ziman (Chap 8 Sec. 5 of Ref. [32]).

Over time, the *dominant coefficients* α have been employed rather loosely, casting confusion on the value to apply to determine the DPW. In the more recent context of nanoscale thermal physics, both $\alpha = 4.25$ and $\alpha = 2.82$ are used, without any reasons justifying why one or the other should be chosen, although these values differ by 50%.

Until now, the DPW has been determined by using only one temperature, generally the regulated cold reservoir temperature of the system. However, in order to get a heat flow, a second heat source is necessary. Therefore, the effective heat flux flowing from the hot reservoir to the cold reservoir depends on the temperatures of both reservoirs. Yet, the effect of the heat flux on the DPW has never been considered before.

Our investigation reveals that for systems subjected to a heat flux, the phonon spectrum is shifted to higher frequencies. As a result, the DPW becomes significantly smaller as the temperature difference between the thermal reservoirs is decreased, a phenomenon we refer to as *blueshift* effect. In the limit of small temperature gradient, we show that not considering the heat flux leads to 62% error in the DPW of 2D materials. We detail the calculations describing the behavior of the DPW in 2D and 3D systems between two thermal reservoirs and provide the corrected dominant coefficient as function of the temperature difference. In the light of our results, we discuss the different DPWs available in literature and show the advantages to work with the phonon energy spectrum. Finally, the dependence of the DPW on temperature differences is shown to notably reduce the thermal conductivity. Thus, the *blueshift* effect alters the physical interpretation of experimental results and can be applied to improve the performances of thermoelectric devices.

II. DPW IN A SINGLE THERMAL RESERVOIR

A. Frequency dependent energy spectrum

The lattice energy associated with a thermal reservoir at a temperature T is given by the general expression[33]

$$E = \sum_m \int_0^{\omega_{max,m}} \left[f_{BE}(\omega, T) + \frac{1}{2} \right] g_m(\omega)\hbar\omega d\omega, \tag{2}$$

where ω is the phonon angular frequency, $f_{BE} = (e^{\hbar\omega/(k_B T)} - 1)^{-1}$ represents the Bose-Einstein distribution and $g_m(\omega) = \omega^2/(2\pi^2 c_m^3)$ denotes the density of states per unit frequency for each phonon propagation mode m characterized at low temperature by a single group velocity $c_m = (d\omega/dk)_m$. The zero-point energy, represented by the 1/2 term in Eq. (2), does not play any role in the heat transfer because it is temperature independent. We conduct the calculations within the framework of the Debye theory for phonons so that ω_{max} corresponds to the Debye angular frequency ω_D and consider a linear dispersion relation $\omega = c_m k$.

The temperature dependent terms under the integral in Eq. (2) define the spectral radiance or spectral energy density per unit frequency: $B_m(\omega, T) = f_{BE}(\omega, T)g_m(\omega)\hbar\omega$. The difference between 2D and 3D systems lies in the density of states. The shape of the spectral energy density is given by $B_m(\omega, T) \propto f_{BE}\omega^3$ and $B_m(\omega, T) \propto f_{BE}\omega^2$ for 3D and 2D, respectively.

The dominant angular frequency ω_d is associated to the peak of $B_m(\omega, T)$. The conversion to wavelengths yields the DPW $\lambda_d = 2\pi c_m/\omega_d = hc_m/(\alpha k_B T)$, which is equivalent to Eq. (1). Letting
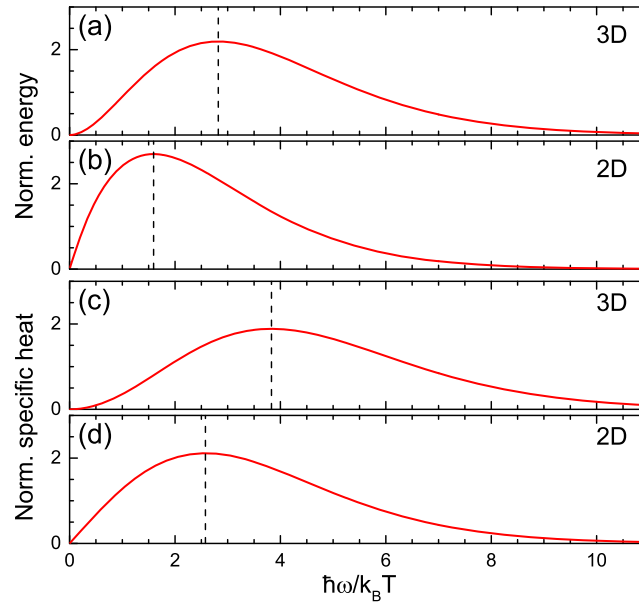
FIG. 1. Normalized phonon spectra. (a) 3D energy spectrum. (b) 2D energy spectrum. (c) 3D specific heat spectrum. (d) 2D specific heat spectrum. The dashed line shows the peak of the distribution.

$X = \hbar\omega/(k_B T)$, $B(\omega, T)$ is normalized such as $\tilde{B}(X) = B(X)/(\int B(X)dX)$. $\tilde{B}(X)$ is plotted in Fig. 1(a). The peak of the spectral energy density is determined numerically with high accuracy to find the value $\alpha = 2.821$ for 3D.

Along the same lines, we derive the 2D energy density spectrum is given Fig. 1(b). Compared to the 3D spectrum, the 2D spectrum is clearly more concentrated at the low frequencies. The dominant coefficient is then significantly reduced to be found for $\alpha = 1.594$.

B. Specific heat distribution

Following the works by Pohl,[12,31] the effective phonons at a given temperature are those that contribute predominantly to the specific heat. Hence, dominant phonon wavelengths can also be determined from the specific heat, which is the temperature derivative of the lattice energy defined in Eq. (2). Therefore, we can define a specific heat density spectrum by $M(\omega, T) = \partial B(\omega, T)/\partial T$. A similar normalization as for the energy leads to the normalized specific heat spectrum $\tilde{M}(X)$ as shown in Fig. 1(c) and (d) for 3D and 2D cases, respectively.

The 3D specific heat spectrum (Fig. 1(c)) is broader than the energy spectrum (Fig. 1(a)) and peaks at higher frequencies with a dominant coefficient $\alpha = 3.830$ while $\alpha = 2.576$ is found for 2D.

The dominant coefficient we have calculated with the energy spectrum and the specific heat spectrum are identical to those given in the introduction and therefore explain the origin of the different DPWs found in the literature. In the case of 3D materials, the experimental value $\alpha = 4.25$, while being a benchmark, seems to point in favor of the specific heat spectrum theory which gives $\alpha = 3.83$. However, the energy spectrum theory, with $\alpha = 2.82$, has also been often chosen. For 2D materials, in the absence of experimental data, the energy spectrum theory has been exclusively used.

III. DPW UNDER HEAT FLUX

The calculations we made in the previous section considered that the thermal properties in a system, 3D or 2D, are given by only one phonon reservoir. However, a heat flow exists only in presence of a temperature difference. We represent this situation by surrounding the system by two reservoirs (see inset Fig.2) and observe the impact of the heat flux on the DPW.

A. Heat flux formalism

First, we consider a 3D thermal reservoir at temperature T. It emits an energy density flux given by:

$$q(T) = \sum_m \int_0^{\omega_{D,m}} B_m(\omega, T) c_m d\omega. \tag{3}$$

For a medium subjected to a temperature gradient due to a hot reservoir at temperature T_h and a cold reservoir at T_c (with $T_c < T_h$), the effective energy density flux flow through the medium is

$$q_{eff}(T_h, T_c) = q_h(T_h) + q_c(T_c), \tag{4}$$

where the hot and cold reservoirs emit a phonon density flux q_h and q_c, respectively. Taking the heat conduction in the direction of the temperature gradient, the orthogonal projection of the velocities on the x axis leads to an effective heat flux given by:

$$q_{eff}(T_h, T_c) = \sum_m \int_0^{\omega_{D,m}} B_m^{eff}(\omega, T_h, T_c) c_{m,x} d\omega, \tag{5}$$

where $B_m^{eff}(\omega, T_h, T_c)$ is the effective energy distribution per mode and is defined by:

$$B_m^{eff}(\omega, T_h, T_c) = B_m(\omega, T_h) - B_m(\omega, T_c). \tag{6}$$

From Eq. (5) and Eq. (6), it is immediately visible that for $T_h = T_c$ there is no heat flux in the system. This situation is similar to the one we describe in Sec. II.

As a supportive example, we represent in Fig. 2 the different terms in Eq. (6) with $T_h = 4.4K$, $T_c = 4.0K$ and by setting $c_m = 6000\, m.s^{-1}$. We clearly observe the displacement of the peak frequency of the effective energy distribution $B_m^{eff}(\omega, T_h, T_c)$ to a higher frequency compared to that of the hot $B_m(\omega, T_h)$ and cold $B_m(\omega, T_c)$ energy distributions. Therefore, phonons contributing predominantly to the effective heat transport have higher frequencies compared to phonons contributing to the peak frequencies of the individual thermal reservoirs. We refer to this shift to higher frequencies as *blueshift* effect. This effect is all the more substantial for smaller heat fluxes, when T_h approaches T_c. Since the cold energy distribution is always overlapped by the hot one, the impact of the cold energy distribution is gradually suppressed as the temperature difference increases between the two
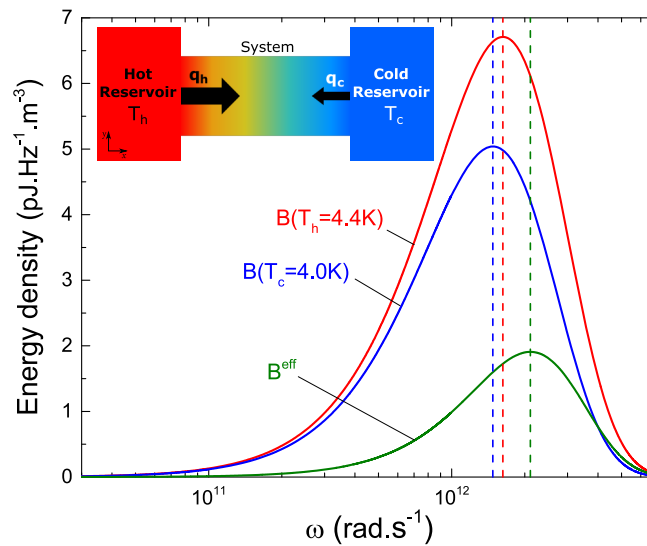

FIG. 2. Spectral energy density of phonons. Red line: $B_m(\omega, T_h)$ for the hot reservoir with $T_h = 4.4K$. Blue line: $B_m(\omega, T_c)$ for the cold reservoir with $T_c = 4.0K$. Green solid line: effective spectral energy density $B_m^{eff}(\omega, T_h, T_c)$. Dashed red, blue and green lines indicate the dominant frequency respectively at $4.4K$, $4.0K$ and the blue-shifted frequency. Inset: Schematic view of the phonons fluxes in a system.

reservoirs. Consequently, the *blueshift* effect is damped until saturation to a constant value for very large temperature differences, as shown later.

To quantify the *blueshift* effect, we determine the peak of the effective energy distribution Eq. (6) by solving the equation (see details in appendix)

$$\frac{1}{e^{\tilde{\theta}_d/T_h} - 1}\left(3 - \frac{\tilde{\theta}_d}{T_h}\frac{e^{\tilde{\theta}_d/T_h}}{e^{\tilde{\theta}_d/T_h} - 1}\right) - \frac{1}{e^{\tilde{\theta}_d/T_c} - 1}\left(3 - \frac{\tilde{\theta}_d}{T_c}\frac{e^{\tilde{\theta}_d/T_c}}{e^{\tilde{\theta}_d/T_c} - 1}\right) = 0, \tag{7}$$

where $\tilde{\theta} = \hbar\omega/k_B$ is a reduced temperature.

The *blueshift* effect can also be observed by considering the specific heat. As in Eq. (5), an effective global specific heat in the system is defined as:

$$C_{eff}(T_h, T_c) = \sum_m \int_0^{\omega_{D,m}} M_m^{eff}(\omega, T_h, T_c)c_{m,x}d\omega, \tag{8}$$

where $M_m^{eff}(\omega, T_h, T_c)$ is the specific heat density spectrum per unit frequency and per mode given by:

$$M_m^{eff}(\omega, T_h, T_c) = \frac{\partial B_m(\omega, T_h)}{\partial T_h} - \frac{\partial B_m(\omega, T_c)}{\partial T_c}. \tag{9}$$

A similar expression as Eq. (7) can then be established by using Eq. (9).

Eq. (6) and Eq. (8) are valid for any dimensionality of the system; only the phonon density of states has to be changed accordingly. Therefore, the concepts we have developed up to now are also applicable to 2D materials.

Actually, we generalized Eq. (7) to encompass the four cases that are the 2D and 3D energy peaks and the 2D and 3D specific heat peaks by taking into account the dimensionality δ of the system that is considered and the order of derivative n with report to the energy distribution. The general equation is given by (see Appendix):

$$\frac{e^{n\tilde{\theta}/T_h}}{T_h^{2n}(e^{\tilde{\theta}/T_h} - 1)}\left[\delta + n + \frac{\tilde{\theta}}{T_h}\left(n - \frac{(n+1)e^{\tilde{\theta}/T_h}}{e^{\tilde{\theta}/T_h} - 1}\right)\right]$$

$$-\frac{e^{n\tilde{\theta}/T_c}}{T_c^{2n}(e^{\tilde{\theta}/T_c} - 1)}\left[\delta + n + \frac{\tilde{\theta}}{T_c}\left(n - \frac{(n+1)e^{\tilde{\theta}/T_c}}{e^{\tilde{\theta}/T_c} - 1}\right)\right]_{\tilde{\theta}=\tilde{\theta}_d} = 0 \tag{10}$$

where $n = 0$ or $n = 1$ when $B_{m,d}^{eff}(\omega, T_h, T_c)$ or $M_{m,d}^{eff}(\omega, T_h, T_c)$ is considered, respectively. The parameter δ is set to 2 or 3 for 2D or 3D systems, respectively. Only the solution of Eq. (10) for which $\tilde{\theta} > 0$ defines the dominant coefficient $\alpha = \tilde{\theta}_d/T_h$.

B. DPW dependence to Δ*T*

Fig. 3(a) shows the spectrum of $\alpha = \tilde{\theta}_d/T_h$ values on a plot of the temperatures of the hot and cold reservoirs, after solving Eq. (10) for $n = 0$ and $\delta = 3$, that is, for a 3D effective energy density distribution. The color scale depicts the evolution of α as a function of T_h and T_c. The linear contour lines passing through the origin displays equal values of α for different T_h/T_c ratios. On the diagonal, $T_h \to T_c$ ($q_{eff} \to 0^+$) and α has a maximum value of $\alpha_0 = 3.830$. As $\Delta T = T_h - T_c$ increases and tends to $T_h \gg T_c$, α decreases to attain a constant value of $\alpha_\infty = 2.821$. In this case the effective heat flux is at its maximum so that $\boldsymbol{q_c}$ is negligible compared to $\boldsymbol{q_h}$ and the situation with a single thermal reservoir is again retrieved.

Fig. 3(b) shows $\tilde{\theta}_d$ as a function of T_h for three different T_h/T_c ratios. Calculations were done with $n = 0$ in Eq. (10); and the $\delta = 3$ and $\delta = 2$ cases are treated for comparison. All datasets indicate a perfect linear dependence between $\tilde{\theta}_d$ and T_h for a constant T_h/T_c ratio. The slope of each curve in Fig. 3(b) represents the dominant coefficient α for a given T_h/T_c ratio. Clearly, α decreases and stabilizes as the temperature differences increase.

Fig. 4 summarizes the behavior of α as a function of for 2D and 3D systems respectively. For each of these cases, the calculations are performed with the effective energy density distribution and with the effective specific heat density distribution for comparison.
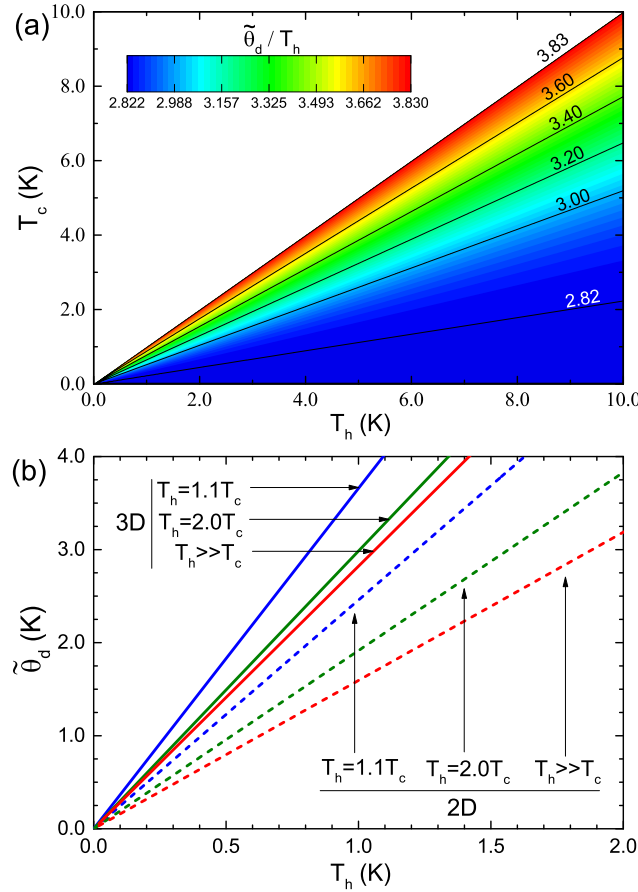
FIG. 3. Evolution of α with T_c and T_h by solving Eq. (10) for the 3D case using the effective energy density distribution. (a) Spectrum of $\alpha = \tilde{\theta}_d / T_h$ shown on a T_h versus T_c map. (b) $\tilde{\theta}_d$ as a function of T_h for different T_c (2D and 3D cases).

All the curves in Fig. 4 have the same exponentially decreasing trend, which we express as:

$$\alpha(T_h, T_c) = \begin{cases} \alpha_\infty + (\alpha_0 - \alpha_\infty)e^{-\gamma \Delta T/T_c} & , \Delta T > 0 \\ \alpha_\infty & , \Delta T = 0 \end{cases} \qquad (11)$$

where α_0 corresponds α values when $\Delta T \to 0^+$ and α_∞ represents either $\Delta T = 0$ or $\Delta T \to \infty$ because these two cases depict the single thermal reservoir situation as mentioned earlier. The γ parameter represents a characteristic decay constant of α from α_0 to α_∞ as $\Delta T/T_c$ increases. From Table I, the γ values for the 3D case are larger than the γ values for the 2D case. Consequently, in 3D systems, the evolution of α is completely damped at $\Delta T/T_c \approx 2$, that is $T_h \to 3T_c$. And, in 2D systems evolution of α persists up to $\Delta T/T_c \approx 3$, that is $T_h \to 5T_c$. All values of α_0 and α_∞ are displayed in Table I. It is interesting to note that the α_∞ values are identical to the α values given in Section II. These results imply that for temperature differences larger than those leading to a constant α value (plateau region in Fig. 4), the contribution of the cold thermal reservoir to the net heat flux can be neglected. Finally, for large temperature differences, we retrieve the configuration of a single reservoir, as discussed in the first part of this paper.

On the other hand, in the limit of small temperature differences, we remark that α_0 for $B^{eff}(\omega, T_h, T_c)$ is identical to α_∞ for $M^{eff}(\omega, T_h, T_c)$ in Table I. This result is logical since the definition of the specific heat is the temperature derivative of the energy. Indeed, a simple Taylor development as $\Delta T \to 0^+$ yields $B^{eff} = M^{eff} \Delta T$. Therefore, the peak of $B^{eff}(\omega, T_h, T_c)$ when $\Delta T = 0^+$ corresponds to the peak of $M^{eff}(\omega, T_h, T_c)$ when $\Delta T \gg 1$. From Eq. (1) and (11), we finally define the general
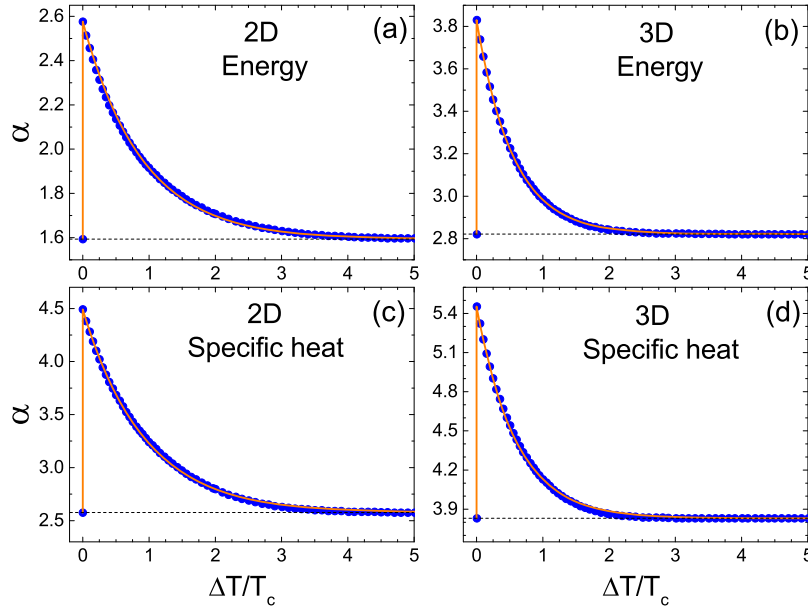
FIG. 4. α as a function of the relative temperature difference $\Delta T/T_C$. Blue dot data were calculated using Eq. (10). The full line is the exponential fit given by Eq. (12) with coefficients given in Table I. The dashed line represents the single thermal reservoir limit. (a) 2D energy. (b) 3D energy. (c) 2D specific heat. (d) 3D specific heat.

TABLE I. Values of the coefficients of Eq. (11) for the energy and specific heat spectra for the 2D and 3D cases.

	2D		3D	
	B^{eff}	M^{eff}	B^{eff}	M^{eff}
α_0	2.576	4.491	3.830	5.452
α_∞	1.594	2.576	2.821	3.830
γ	1.119	1.078	1.830	1.689

expression of the DPW, including the blueshift effect as

$$\lambda_d = \frac{hc}{\alpha(T_h, T_c)k_B T_h},\tag{12}$$

The relative difference between α_0 and α_∞ compared to α_∞ is ~62% in the 2D case and ~36% in 3D case. These percentages represent the maximum error that can be committed by ignoring the effective heat flux. The increase of α demonstrated Eq. (11) has a direct consequence to lower λ_d, and therefore to induce a frequency blueshift. This blueshift is all the more important in thermal experiments because the relative temperature difference is generally maintained under 10% in order to avoid non-linear effects.[34] This region of small $\Delta T/T_c$ is precisely where the blueshift is the strongest because of the exponential decay form. For example, if we consider the energy spectrum in Fig. 4(b) for the 3D case, we see that a $\Delta T/T_c = 0.1$ leads to $\alpha \approx 3.66$ which is ~30% above the widely used value of 2.82 corresponding to the peak of the energy density distribution.

C. Comment on the use of the energy spectrum

The only experimental value of the DPW was given by Pohl who deduced $\alpha = 4.25$ thanks to low temperature thermal conductivity measurements.[31] Taking into account the 10% experimental error, this value was then attributed to the peak of the specific heat spectrum[12] which theoretically yields $\alpha = 3.83$.

Thermal conductivity measurements requires the presence of a heat flux in the material. The experimental value of α can therefore be also interpreted as a manifestation of the *blueshift* effect.

Indeed, in the small heat flux limit, we have demonstrated that the energy spectrum also leads to $\alpha = 3.83$ which is in agreement with the measurements.

The parallel between phonon and photon makes possible their common physical treatment as part of the boson family. As for photons, only the energy spectrum is used.[35,36] Finally, as the *blueshift* effect reconciles the experiment and the energy theoretical value, we would recommend to use the energy spectrum to determine the DPW.

D. Blueshift effect on the thermal conductivity

In the boundary scattering regime, the mean free path of phonons is strongly affected by phonon-surface roughness interactions.[11] The nature of these interactions is determined by a specularity factor which represents the fraction of total number of phonons undergoing specular scattering; and it is given, according to Ziman's formula,[32] by $p(\sigma, \lambda) = \exp(-16\pi^2\sigma^2/\lambda^2)$, where σ is the surface roughness height. A surface for which $\sigma \gg \lambda$ is defined as perfectly rough and phonon scattering is fully diffusive, that is $p(\sigma, \lambda) = 0$. Casimir[37] defines the thermal conductivity under these conditions to be written as: $\kappa_{diff} = C_p c \Lambda_{diff}/3$, where Λ_{diff} is the mean free path of the diffusive phonons.

When both specular and diffuse scattering are present, the effective mean free path is given as

$$\Lambda_{eff} = \frac{1 + \bar{p}(\lambda_d)}{1 - \bar{p}(\lambda_d)}\Lambda_{diff}, \tag{13}$$

where $\bar{p}(\lambda_d)$ is the average specularity parameter. Ziman showed that it depends on λ_d following the integral[32]

$$\bar{p}(\lambda_d) \approx \int_0^{\lambda_d/4} P(\sigma)d\sigma = 1 - \exp\left(-\frac{\lambda_d}{4\pi\sigma_0}\right). \tag{14}$$

The distribution of roughnesses $P(\sigma)$ we use in Eq. 14 was determined experimentally by Heron et al[18] as $P(\sigma) = e^{-\sigma/\sigma_0}$ where σ_0 is the root mean square surface roughness. Inserting Eq. (12) into Eq. (14), the blueshift effect decreases the average specularity parameter and so reduce the effective mean free path.

The impact of the *blueshift* effect on the thermal conductivity is assessed by using Eq. (13) which directly leads to the $\kappa_{eff}/\kappa_{diff}$ ratio. Fig. 5 shows this ratio as a function of temperature for a 3D structure with a root mean square roughness $\sigma_0 = 4nm$. For a given cold temperature T_c, the $\kappa_{eff}/\kappa_{diff}$ ratio has a maximum value when the system is at thermal equilibrium $\Delta T/T_c = 0$ (which also corresponds to the single thermal reservoir case). This situation is represented by the dashed line. The lower limit, pictured by the full line, is obtained when the *blueshift* is maximum which is attained
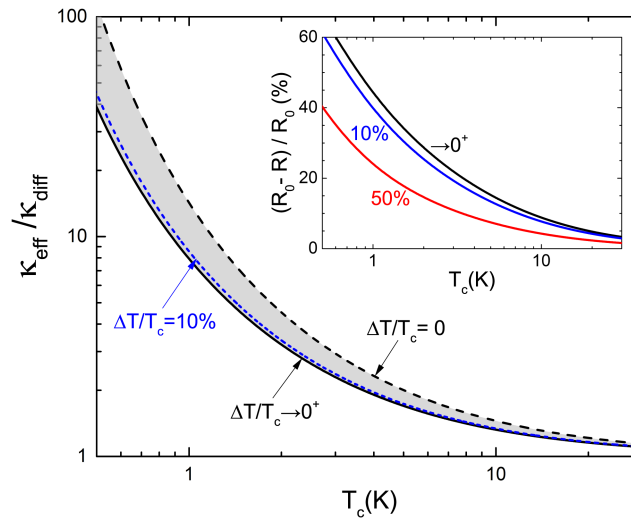

FIG. 5. $\kappa_{eff}/\kappa_{diff}$ calculated by using the DPW for the 3D energy distribution and a roughness $\sigma_0 = 4nm$ as a function of temperature for different $\Delta T/T_c$. The inset shows the relative difference of the $R = \kappa_{eff}/\kappa_{diff}$ ratio at a given $\Delta T/T_c$, compared to the R_0 ratio at thermal equilibrium.

when the temperature difference tends to zero $\Delta T/T_c \to 0^+$, without being strictly equal to zero. Among all the intermediate relative temperature differences, we plot the special case $\Delta T/T_c = 10\%$, which corresponds to the conventional upper limit to avoid non-linear heat flux effects, with a blue dotted line. The results clearly indicate a decreasing effective thermal conductivity due to a reduction of the DPW caused by the *blueshift* effect.

The inset in Fig. 5 shows the relative difference in percentage between the $R = \kappa_{eff}/\kappa_{diff}$ ratio at a given $\Delta T/T_c$ and $R_0 = \kappa_{eff}/\kappa_{diff}$ for $\Delta T/T_c = 0$ at thermal equilibrium. For $\Delta T/T_c = 10\%$, the observed reduction exceeds 20% below 4K showing the importance of the *blueshift* effect at low temperature. As the temperature increases the relative difference decreases because of the transition from the semi-ballistic regime to the diffusive regime. Consequently, the impact of the *blueshift* is below 5% above 20K.

High performance thermoelectric modules are important for cooling electronic circuits in quantum computing and superconducting devices.[38] The performances of thermoelectric devices can be improved by two ways thanks to the *blueshift* effect by choosing the correct thermal environment. Firstly, thermoelectric devices working according to incoherent thermal transport principles, e.g. rough nanowires,[39] should be placed under low heat flux conditions. Following the above discussion, a smaller temperature difference yields a smaller thermal conductivity, thereby increasing the thermoelectric figure of merit. Secondly, phononic crystals, where partially coherent thermal transport occurs, should be placed under high heat flux. Indeed, it has been recently shown that the periodic pattern of phononic crystals creates interference of coherent phonons by Bragg diffraction, thus hindering heat propagation.[40] The higher the heat flux, the higher the DPW which leads to a higher proportion of coherent phonons finally providing a lower thermal conductivity. However, increasing the heat flux in a structure has also an impact which decreases the DPW because of the temperature increase. The temperature difference in the structure, while relatively large, has therefore to remain limited. As reported in Fig. 4, maximum performances of thermoelectric phononic crystals should be attained for $\Delta T/T_c \sim 3$ in 2D materials and ~ 2 in 3D materials. Finally, we note that in Ref. 11 we give the relationship between sample size and temperature for boundary scattering to predominate.

IV. CONCLUSION

Having established and consolidated the definitions of DPW, we then studied its evolution induced by a heat flux imposed by two thermal reservoirs. We show that the effective energy and specific heat density distributions describing the system undergo a shift to higher frequencies that is controlled by the temperatures of the two thermal reservoirs. Consequently, the *blueshift* effect now leads to the dominant coefficient α to vary as a function of the temperature difference. We have established that the DPW is reduced as the heat flux decreases, following an exponential decay law. This reduction is substantial as it can reach up to ~62% for 2D systems and ~36% for 3D systems.

The impact of the DPW shift on the thermal conductivity has been studied via the phonon mean free path which depends on the average specularity parameter $\bar{p}$. The results clearly show that the relative change in the thermal conductivity $\kappa_{eff}/\kappa_{diff}$ decreases by more than 20% at 4K for temperature differences as small as 10%. It indicates that an adequate heat flux environment can improve the performances of thermoelectric devices. Besides, the misjudgment on the thermal conductivity by ignoring the *blueshift* effect can significantly alter the physical interpretation of experimental results.

Our calculations provide a ready-to-use formula to determine the dominant phonon wavelength. It serves as a useful and immediately available reference especially for nanostructured materials where effects such as confinement or thermal rectification may operate. Experimental measurements of the decay constant γ in the expression for α may help to corroborate our predictions of the *blueshift* effect in presence of a heat flux.

APPENDIX

This appendix presents the details of the derivation of the DPW expressions Eq. (7) in the 3D energetic case and its generalization to 2D and 3D with the specific heat given Eq. (10).

The 3D spectral density of energy in the Debye approximation can be written as

$$B_m(\omega, T) = \frac{\hbar}{2\pi^2 c_m^3} \frac{\omega^3}{e^{\hbar\omega/(k_B T)} - 1}, \tag{A.1}$$

which yields the effective spectral density of energy

$$B_m^{eff}(\omega, T_h, T_c) = \frac{3\hbar^2\omega^3}{2\pi^2 c_m^3} \left(\frac{1}{e^{\hbar\omega/(k_B T_h)} - 1} - \frac{1}{e^{\hbar\omega/(k_B T_c)} - 1} \right). \tag{A.2}$$

Letting $\tilde{\theta} = \hbar\omega/k_B$ and inserting it in Eq. (A.2) gives:

$$B_m^{eff}(\tilde{\theta}, T_h, T_c) \propto \tilde{\theta}^3 \left(\frac{1}{e^{\tilde{\theta}/T_h} - 1} - \frac{1}{e^{\tilde{\theta}/T_c} - 1} \right). \tag{A.3}$$

Coefficients that only change the amplitude of the spectrum but do not affect the position of its maximum have been removed from Eq. (A.3). The derivative with respect to $\tilde{\theta}$ leads to:

$$\frac{\partial B_m^{eff}(\tilde{\theta}, T_h, T_c)}{\partial \tilde{\theta}} = 3\tilde{\theta}^2 \left(\frac{1}{e^{\tilde{\theta}/T_h} - 1} - \frac{1}{e^{\tilde{\theta}/T_c} - 1} \right) + \tilde{\theta}^3 \left[\frac{e^{\tilde{\theta}/T_c}/T_c}{(e^{\tilde{\theta}/T_c} - 1)^2} - \frac{e^{\tilde{\theta}/T_h}/T_h}{(e^{\tilde{\theta}/T_h} - 1)^2} \right] \tag{A.4}$$

By definition of the peak, Eq. (A.4) is equal to zero when $\tilde{\theta} = \tilde{\theta}_d$, so

$$3\left(\frac{1}{e^{\tilde{\theta}_d/T_h} - 1} - \frac{1}{e^{\tilde{\theta}_d/T_c} - 1} \right) + \tilde{\theta}_d \left[\frac{e^{\tilde{\theta}_d/T_c}/T_c}{(e^{\tilde{\theta}_d/T_c} - 1)^2} - \frac{e^{\tilde{\theta}_d/T_h}/T_h}{(e^{\tilde{\theta}_d/T_h} - 1)^2} \right] = 0 \tag{A.5}$$

We separate the terms with the hot temperature T_h from those with T_c to find a symmetrical form identical to Eq. (7):

$$\frac{1}{e^{\tilde{\theta}_d/T_h} - 1} \left(3 - \frac{\tilde{\theta}_d}{T_h} \frac{e^{\tilde{\theta}_d/T_h}}{e^{\tilde{\theta}_d/T_h} - 1} \right) - \frac{1}{e^{\tilde{\theta}_d/T_c} - 1} \left(3 - \frac{\tilde{\theta}_d}{T_c} \frac{e^{\tilde{\theta}_d/T_c}}{e^{\tilde{\theta}_d/T_c} - 1} \right) = 0 \tag{A.6}$$

We follow the same steps for the 3D specific heat, starting with Eq. (9):

$$M_m^{eff}(\tilde{\theta}, T_h, T_c) \propto \tilde{\theta}^4 \left(\frac{e^{\tilde{\theta}/T_h}}{(e^{\tilde{\theta}/T_h} - 1)^2} - \frac{e^{\tilde{\theta}/T_c}}{(e^{\tilde{\theta}/T_c} - 1)^2} \right) \tag{A.7}$$

Then the derivative yields

$$\frac{\partial M_m^{eff}(\tilde{\theta}, T_h, T_c)}{\partial \tilde{\theta}} = 4\tilde{\theta}^3 \left[\frac{e^{\tilde{\theta}/T_h}}{T_h^2(e^{\tilde{\theta}/T_h} - 1)^2} - \frac{e^{\tilde{\theta}/T_c}}{T_c^2(e^{\tilde{\theta}/T_c} - 1)^2} \right]$$

$$+ \tilde{\theta}^4 \left[\frac{e^{\tilde{\theta}/T_h}}{T_h^3(e^{\tilde{\theta}/T_h} - 1)^2} \left(1 - \frac{2e^{\tilde{\theta}/T_h}}{e^{\tilde{\theta}/T_h} - 1} \right) \right.$$

$$\left. - \frac{e^{\tilde{\theta}/T_c}}{T_h^3(e^{\tilde{\theta}/T_c} - 1)^2} \left(1 - \frac{2e^{\tilde{\theta}/T_c}}{e^{\tilde{\theta}/T_c} - 1} \right) \right] \tag{A.8}$$

It is now straightforward to write the equation to find the maximum

$$\frac{e^{\tilde{\theta}/T_h}}{T_h^2(e^{\tilde{\theta}/T_h} - 1)} \left[4 + \frac{\tilde{\theta}}{T_h} \left(1 - \frac{2e^{\tilde{\theta}/T_h}}{e^{\tilde{\theta}/T_h} - 1} \right) \right]$$

$$- \frac{e^{\tilde{\theta}/T_c}}{T_c^2(e^{\tilde{\theta}/T_c} - 1)} \left[4 + \frac{\tilde{\theta}}{T_c} \left(1 - \frac{2e^{\tilde{\theta}/T_c}}{e^{\tilde{\theta}/T_c} - 1} \right) \right] = 0 \tag{A.9}$$

By introducing n as the temperature derivative order of $B_m^{eff}(\omega, T_h, T_c)$ ($n = 0$ for the energy and $n = 1$ for the specific heat), Eq. (A.6) and Eq. (A.9) are unified as a single expression similar to Eq. (10) (with $\delta = 3$).

The complete generalization Eq. (10) is made by noticing that the 3D spectral density of energy expression Eq. (A.1) can be extended to incorporate the 2D case by introducing the dimensionality parameter δ as follow

$$B_{m,\delta}(\omega, T) = \frac{\hbar}{2\pi^{\delta-1}c_m^{\delta}} \frac{\omega^{\delta}}{e^{\hbar\omega/(k_B T)} - 1} \tag{A.10}$$

The same derivation line is then implemented for 2D systems.

[1] D. G. Cahill, P. V. Braun, G. Chen, D. R. Clarke, S. Fan, K. E. Goodson, P. Keblinski, W. P. King, G. D. Mahan, A. Majumdar, H. J. Maris, S. R. Phillpot, E. Pop, and L. Shi, Appl. Phys. Rev. **1**, 11305 (2014).

[2] N. Yang, X. Xu, G. Zhang, and B. Li, AIP Adv. **2**, 41410 (2012).

[3] A. M. Marconnet, M. Asheghi, and K. E. Goodson, J. Heat Transfer **135**, 061601 (2013).

[4] A. A. Balandin, S. Ghosh, W. Bao, I. Calizo, D. Teweldebrhan, F. Miao, and C. N. Lau, Nano Lett. **8**, 902 (2008).

[5] J. H. Seol, I. Jo, A. L. Moore, L. Lindsay, Z. H. Aitken, M. T. Pettes, X. Li, Z. Yao, R. Huang, D. Broido, N. Mingo, R. S. Ruoff, and L. Shi, Science **328**, 213 (2010).

[6] X. Zhang, H. Xie, M. Hu, H. Bao, S. Yue, G. Qin, and G. Su, Phys. Rev. B **89**, 54310 (2014).

[7] M. N. Luckyanova, J. Garg, K. Esfarjani, A. Jandl, M. T. Bulsara, A. J. Schmidt, A. J. Minnich, S. Chen, M. S. Dresselhaus, Z. Ren, E. A. Fitzgerald, and G. Chen, Science **338**, 936 (2012).

[8] C. L. Poyser, T. Czerniuk, A. Akimov, B. T. Diroll, E. A. Gaulding, A. S. Salasyuk, A. J. Kent, D. R. Yakovlev, M. Bayer, and C. B. Murray, ACS Nano **10**, 1163 (2016).

[9] B. Latour, S. Volz, and Y. Chalopin, Phys. Rev. B **90**, 014307 (2014).

[10] J. H. Oh, M. Shin, and M.-G. Jang, J. Appl. Phys. **111**, 44304 (2012).

[11] A. Ramiere, S. Volz, and J. Amrit, J. Phys. D: Appl. Phys. **49**, 115306 (2016).

[12] T. Klitsner and R. Pohl, Phys. Rev. B **36**, 6551 (1987).

[13] C. Blanc, A. Rajabpour, S. Volz, T. Fournier, and O. Bourgeois, Appl. Phys. Lett. **103**, 043109 (2013).

[14] M. G. Ghossoub, K. V. Valavala, M. Seong, B. Azeredo, K. Hsu, J. S. Sadhu, P. K. Singh, and S. Sinha, Nano Lett. **13**, 1564 (2013).

[15] V. Jean, S. Fumeron, K. Termentzidis, X. Zianni, and D. Lacroix, Int. J. Heat Mass Transfer **86**, 648 (2015).

[16] O. Bourgeois, T. Fournier, and J. Chaussy, J. Appl. Phys **101**, 016104 (2007).

[17] R. Prasher, T. Tong, and A. Majumdar, Nano Lett. **8**, 99 (2008).

[18] J. S. Heron, T. Fournier, N. Mingo, and O. Bourgeois, Nano Lett. **9**, 1861 (2009).

[19] T. Nakayama, Prog. Low Temp. Phys. **12**, 115 (1989).

[20] J. Amrit and M. X. François, J. Low Temp. Phys. **128**, 113 (2002).

[21] J. Amrit, Phys. Rev. B **81**, 54303 (2010).

[22] A. Ramiere, S. Volz, and J. Amrit, Nature Mater. **15**, 512 (2016).

[23] R. Chen, A. I. Hochbaum, P. Murphy, J. Moore, P. Yang, and A. Majumdar, Phys. Rev. Lett. **101**, 105501 (2008).

[24] M. Nomura, J. Nakagawa, Y. Kage, J. Maire, D. Moser, and O. Paul, Appl. Phys. Lett. **106**, 143102 (2015).

[25] K. Schwab, J. L. Arlett, J. M. Worlock, and M. L. Roukes, Physica E **9**, 60 (2001).

[26] L. Sun and J. Y. Murthy, Appl. Phys. Lett. **89**, 171919 (2006).

[27] N. Zen, T. A. Puurtinen, T. J. Isotalo, S. Chaudhuri, and I. J. Maasilta, Nat. Commun. **5** (2014).

[28] D. Anghel, J. Pekola, M. Leivo, J. Suoknuuti, and M. Manninen, Phys. Rev. Lett. **81**, 2958 (1998).

[29] L. G. C. Rego and G. Kirczenow, Phys. Rev. Lett. **81**, 232 (1998).

[30] S. Alaie, D. F. Goettler, M. Su, Z. C. Leseman, C. M. Reinke, and I. El-Kady, Nat. Commun. **6**, 7228 (2015).

[31] R. O. Pohl, in *Elementary excitations in solids*, edited by A. A. Mradudin and G. F. Nardelli (Plenum Press, 1969), p. 259.

[32] J. M. Ziman, *Electrons and Phonons*, edited by The International series of monographs on physics (Oxford University Press, 1960).

[33] C. Kittel, *Introduction to Solid State Physics*, 8th ed. (John Wiley & Sons, 2004).

[34] S. W. Van Sciver, *Helium Cryogenics* (Plenum Press, 1986).

[35] J. M. Marr and F. P. Wilkin, Am. J. Phys. **80**, 399 (2012).

[36] D. W. Ball, J. Chem. Educ. **90**, 1250 (2013).

[37] H. B. G. Casimir, Physica **5**, 495 (1938).

[38] D.-Y. Chung, T. Hogan, P. Brazis, M. Rocci-Lane, C. Kannewurf, M. Bastea, C. Uher, and M. G. Kanatzidis, Science **287**, 1024 LP (2000).

[39] A. I. Hochbaum, R. Chen, R. D. Delgado, W. Liang, E. C. Garnett, M. Najarian, A. Majumdar, and P. Yang, Nature **451**, 163 (2008).

[40] M. R. Wagner, B. Graczykowski, J. S. Reparaz, A. E. Sachat, M. Sledzinska, F. Alzina, and C. M. S. Torres, Nano Lett. **9**, 5661 (2016).